Geometry-controlled droplet generation in head-on microfluidic devices

Lingling Shui,[1,a] Frieder Mugele,[2] Albert van den Berg,[1] and Jan C. T. Eijkel[1]
[1]*BIOS/Lab-on-a-Chip Group, MESA+Institute for Nanotechnology, University of Twente, 7500AE, Enschede, The Netherlands*
[2]*Physics of Complex Fluids, Department of Science and Technology, University of Twente, 7500AE, Enschede The Netherlands*

(Received 29 July 2008; accepted 17 September 2008; published online 16 October 2008)

We investigated the generation of droplets in a head-on microfluidic device operated with the two identical channels as inlets and the "long leg" as a constriction channel leading to a wider outlet section. For capillary numbers (Ca) of approximately 10^{-5} or less, we find a Ca-independent droplet volume equal to the volume of the constriction channel, which decreases at higher Ca when shear forces become relevant. The droplet generation mechanism is explained in terms of a global capillary instability involving surprisingly stable intermediate surface configurations. © *2008 American Institute of Physics*. [DOI: 10.1063/1.3000624]

Droplet-based multiphase microfluidics is rapidly becoming an important area in microfluidics with many possible applications for chemical and biological purposes.[1,2] The creation of monodisperse droplets is one of the most important requirements for many of these applications. The most commonly used geometries for two-phase flow are T-junctions[3–5] and flow-focusing devices.[6,7] Experiments have mostly been performed in microchannels fabricated in polydimethylsiloxane (PDMS) where water droplets in oil phase were obtained due to the hydrophobicity of PDMS. However, the permeability and deformability of PDMS prevents investigators from using extremely low or high flow rates. Generally, flow rates corresponding to capillary numbers (Ca) of $10^{-3}-1$ have been investigated.[3,7] ($\mathrm{Ca}=\eta v/\sigma$, where η and v are the viscosity and average flow velocity of the continuous phase, respectively, and σ is the interfacial tension[5,8]). Microfluidic droplet generation is therefore affected by shear forces in these geometries under these conditions.

In the present paper, we are interested in droplet generation at extremely low Ca numbers in "head-on devices" consisting of two identical channels as inlets and the "long leg" as a constriction channel leading to a wider outlet section, as shown in Fig. 1. Microchannels were fabricated in silicon-glass using standard photolithography with homogeneous and regular cross sections. Chips were placed in a homemade chip holder, which can easily be connected to gas-tight syringes (Hamilton) using nanoport connectors (Upchurch Scientific). Water [de-ionized water with 0.01*M* sodium dodecyl sulfate (SDS) and 0.01*M* fluorescein sodium salt, $\eta=10^{-3}$ Pa s] and oil (hexadecane, $\eta=3\times10^{-3}$ Pa s) phases were pumped using a syringe pump (Harvard PHD 22/2000). The water-hexadecane interfacial tension with SDS is 0.01 N m^{-1}. Flow rates (Q) were varied between $10^{-3}-1$ μl/min corresponding to $\mathrm{Ca}=10^{-7}-10^{-3}$. Water flows as continuous phase and oil as dispersed phase due to the channel hydrophilicity. The flow was visualized using an inverted microscope (Leica DMIRM) and recorded by using a charge-coupled device camera (Orca ER).

Figure 2 illustrates the typical droplet formation process. An oil thread advances along the constriction channel toward the outlet region. Its tip is separated by a short (bright) water slug from the previous thread. The oil thread is separated from the channel walls by the continuous water phase. The presence of the water is clearly visible at the edges of the channel, where a wetting corner film gives rise to enhanced fluorescence signal in the pictures. As the oil thread advances, its cross-sectional shape remains constant from the junction area to the tip. In the junction area, an oil-water interface with a constant in-plane curvature of order $2/w$ connects the oil in the inlet channel to the oil thread in the constriction channel. Once the tip reaches the wider outlet channel, it expands and begins to form a droplet. Nearly simultaneously, the oil thread in the junction area becomes thinner and thinner and eventually breaks. Subsequently, the

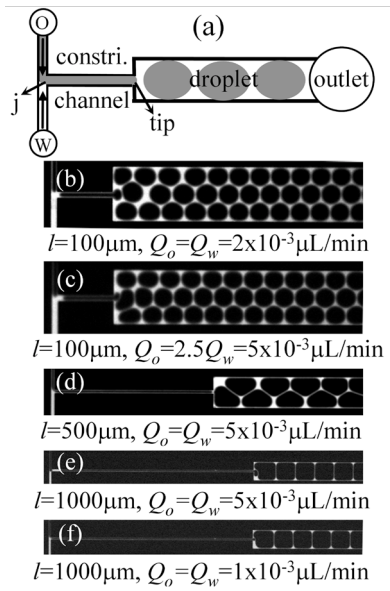

FIG. 1. (Color online) (a) Sketch of the head-on configuration. j and tip indicate junction and oil tip areas, respectively. The channel depth (h) is either 10 or 20 μm. Outlet channel width (W) is 100 μm. Two identical inlet channels are 10×10 or 20×20 $\mu\mathrm{m}^2$. Constriction channels lengths (l) are 100, 400, 500, or 1000 μm and widths (w) are 10, 20, or 40 μm. [(b)–(f)] Snapshots of the geometrically induced droplet formation in different devices and at different flow rate and flow rate ratios.

[a]Electronic mail: l.shui@ewi.utwente.nl.

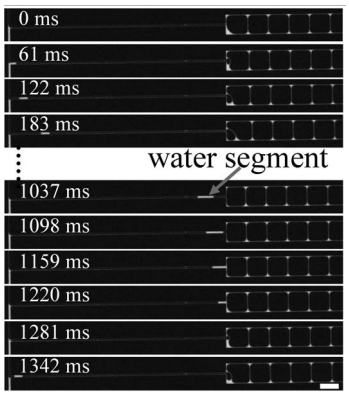

FIG. 2. The process of droplet generation: $h=10\ \mu$m, $w=10\ \mu$m, and $l=1000\ \mu$m (Ref. 13). The scale bar is 100 μm.

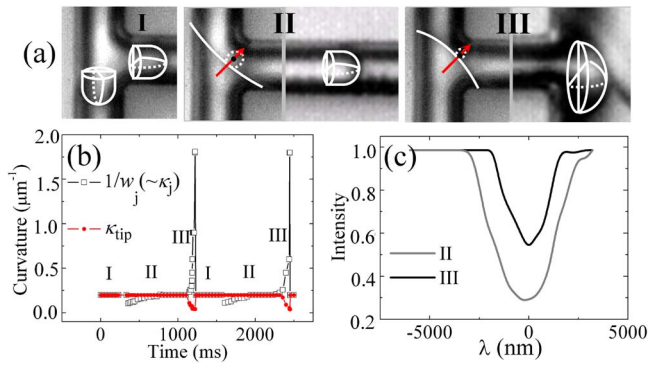

FIG. 4. (Color online) (a) The shapes of the oil thread in the junction and tip areas at different stages, visualized in transmitted light. (b) The mean curvature of the oil thread in the junction ($\kappa_j \approx 1/w_j$, w_j is the smallest oil thread width across the junction) and tip (κ_{tip}) areas vs time, $h=10\ \mu$m, $w=10\ \mu$m, and $l=500\ \mu$m. (c) The fluorescence intensity profile measured across the oil thread center in the junction area at stages II and III (arrows). λ is the distance to the oil thread center. Intensity values are in arbitrary units normalized to the fluorescent intensity in the water inlet channel.

rest of the now disconnected thread advances through the constriction channel and produces the droplet. Figures 3(a) and 3(b) show the volume (V) of the droplets formed in this manner for several channel geometries as a function of Ca. It turns out that V is independent of Ca below a certain channel-dependent threshold value Ca_c. The final droplet volume is thereby almost exactly given by the volume of the constriction channel provided that the latter is sufficiently long. This is demonstrated in Fig. 3(c), where we plotted the obtained droplet volume (experimental results) in units of the constriction channel volume (theoretical values). The droplet volume is thus determined in a very robust fashion by the design of the channel geometry.

We now focus on two aspects of the process described above: (i) the flow pattern of the coflowing oil and water phases and (ii) the stability and breakup mechanism of the oil phase in the junction area.

Let us first consider the flow regime. Operating in the regime of low Ca, we expect viscous forces to be negligible. This can be verified explicitly by comparing the hydrodynamic pressure drop ΔP_H in the system to the characteristic Laplace pressure ΔP_L, which is of order σ/w. Assuming laminar flow, the pressure drop following Hagen–Poiseuille can be simply expressed as $\Delta P_H \approx \eta LQ/d^4$, with L the length of the emerging droplet and d a characteristic dimension.[9] Inserting typical numbers, we find that $\Delta P_H = O(10\ \text{Pa})$, while, $\Delta P_L = O(10^4\ \text{Pa})$ Hence, the viscous pressure drop can indeed be neglected. Under these conditions, the quasistatic oil-water interface has to obey the constraint of constant mean curvature.

Since the mean curvature of the tip of the oil thread is given by $\kappa_{tip}=(2/h+2/w)/2$, the cross-sectional area of the oil thread behind the tip has to be of rectangular shape with rounded corners[10] (see Fig. 5), with the curvature in the corners (κ_{corn}) corresponding to the tip curvature (κ_{tip}), $\kappa_{corn}=\kappa_{tip}$. [Between these rounded corners, there will be a microscopically thin water film at very low flow rate ($Ca^{2/3} \ll 1$), which we neglect for the purposes of this work.] The water flows parallel with the oil thread, in the corners taking a fillet shape. Apart from generating fluorescence along the channel edge, the presence of the coflowing water manifests itself also in both the speed of the advancing oil tip as well as the size of the water slugs separating two consecutive oil threads in the constriction channel. The oil thread tip moves typically about 10% faster than expected if based on the volume flow rate with the simple single phase Poiseuille flow for a rectangular channel. The length of the water slug is found to increase as it travels down the constriction channel, showing that the continuous phase flows past the oil thread like in a leaky piston.[11] These observations are in line with the imposed water flow rate and the requirement of volume conservation, as indicated earlier by others.

What determines the breakup of the capillary bridge in the junction area and its stability prior to breakup? Figure 4(a) shows the typical evolution of the oil thread in the junction and tip areas in a device where $w=h=10\ \mu$m. As discussed above, the oil-water interface has a constant mean curvature—given by κ_{tip}—at all times (except immediately prior to pinch off). In the junction area, a transient stage I occurs in the beginning when the oil bulges into the water

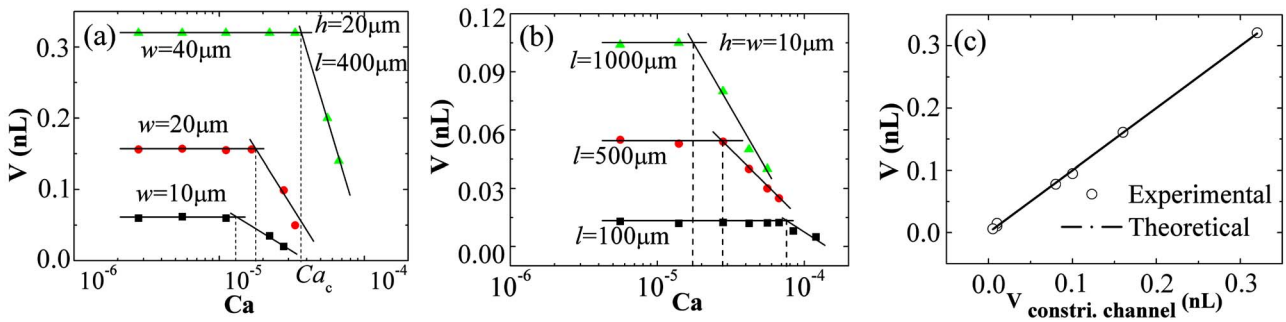

FIG. 3. (Color online) V vs Ca in different devices: (a) varied w at $h=20\ \mu$m and $l=400\ \mu$m, and (b) varied l at $h=w=10\ \mu$m. The dash lines indicate Ca_c. Here $Q_w=Q_o$. (c) V vs $V_{constrchannel}$ (theoretical constriction channel volume) in different devices.

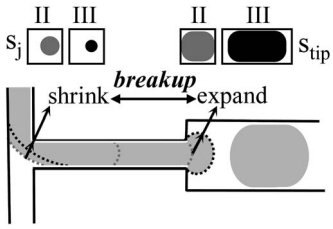

FIG. 5. Schematic of the droplet formation mechanism in stage II and III. Cross sections through the oil thread in the junction area (S_j) at its narrowest point and through the oil tip at its widest point (S_{tip}) are sketched. Measurements (Fig. 4) indicate the detachment of the oil thread from the confining walls and its narrowing in stage III.

channel [Fig. 4(a) I] giving a local mean curvature equals to κ_{tip}. When stage II commences, the oil retreats to form a thread running through the junction area. In stages II and III, the in-plane curvature (solid line) is negligible compare to the out-of-plane curvature (dotted line), as shown in Fig. 4(a) II. The mean curvature in the junction area can then be approximated by the local oil thread width: $\kappa_j \approx 1/w_j$. Open squares and solid circles in Fig. 4(b) compare $1/w_j$ ($\sim\kappa_j$) in stage II and III with κ_{tip}. As expected $1/w_j$ is equal to κ_{tip} most of the time, while the oil thread advances along the constriction channel ($\sim$0.7 s for the data shown here), except for a short phase between stage I and II, when the in-plane curvature can not be neglected. The equality of $1/w_j$ ($\sim\kappa_j$) and κ_{tip} in stage II implies that $w_j=h/2$. To retain a circular cross section means that the oil thread is detached from the channel walls. This is indeed confirmed by the fluorescence profile as measured across the oil thread in the junction area [Fig. 4(c)]. At first glance, one might be surprised that such a thin thread is stable for such a long time since it should break up within approximately 0.01–0.1 s following the Rayleigh plateau instability scenario. However, unlike the classical Rayleigh plateau instability, the oil thread in our present experiments is not part of a free jet but connected to the oil threads in the inlet and the constriction channels, respectively. The channel wall confinement now stabilizes the thin oil thread in the junction area[12] (see Fig. 5 and Ref. 13). Once the tip reaches the wider outlet region (stage III), it expands as described above, leading to a sudden decrease of the local pressure. Owing to the finite imposed oil flow rate and the hydrodynamic resistance in the junction area, this leads to the breakup of the oil thread in this area. The breakup process takes between 10 and 100 ms, depending on the cross section of the constriction channel and the flow rate. During that time, liquid still flows from the inlet channel through the junction into the forming droplet. As a consequence, the final droplet volume is slightly larger than the constriction channel volume.

In summary, we found that the generation of oil droplets in a head-on two-phase microfluidic device for Ca numbers of 10^{-5} and less is controlled by the geometry of the device and the resulting Laplace pressure. Confinement due to the channel walls leads to the stabilization of otherwise unstable liquid morphologies.

We gratefully acknowledge Professor G. M. Homsy and Sumita Pennathur for helpful discussions, and Daniel Wijnperle for assistance with fabrication of devices. This research was supported by the Dutch Ministry of Economic Affairs through a Nanoimpuls grant.

[1] A. van den Berg and T. S. J. Lammerink, Top. Curr. Chem. **194**, 21 (1997).
[2] L. Shui, J. C. T. Eijkel, and A. van den Berg, Adv. Colloid Interface Sci. **133**, 35 (2007).
[3] P. Garstecki, M. J. Fuerstman, H. A. Stone, and G. M. Whitesides, Lab Chip **6**, 437 (2006).
[4] J. D. Tice, A. D. Lyon, and R. F. Ismagilov, Anal. Chim. Acta **507**, 73 (2004).
[5] J. D. Tice, H. Song, A. D. Lyon, and R. F. Ismagilov, Langmuir **19**, 9127 (2003).
[6] R. Dreyfus, P. Tabeling, and H. Willaime, Phys. Rev. Lett. **90**, 144505 (2003).
[7] P. Garstecki, I. Gitlin, W. DiLuzio, G. M. Whitesides, E. Kumacheva, and H. A. Stone, Appl. Phys. Lett. **85**, 2649 (2004).
[8] B. Zheng, J. D. Tice, and R. F. Ismagilov, Anal. Chem. **76**, 4977 (2004).
[9] A. Aota, A. Hibara, and T. Kitamori, Anal. Chem. **79**, 3919 (2007).
[10] V. S. Ajaev and G. M. Homsy, J. Colloid Interface Sci. **244**, 180 (2001).
[11] E. Lajeunesse and G. M. Homsy, Phys. Fluids **15**, 308 (2003).
[12] We rationalize the stabilization as follows. The fastest growing unstable modes in the classical Rayleigh plateau instability distribute the liquid only on a local scale, i.e., they would force liquid from the junction area into the entrance of the adjacent constriction channel. Such a perturbation, however, would experience a restoring force because it requires forcing the liquid-liquid interface further into the corners. As a consequence, such perturbations are no longer unstable and the breakup can only occur through slower nonlocal perturbations. Note that this picture is also different from the convective stabilization of confined jets discussed by P. Guillot, Phys. Rev. Lett. **99**, 104502 (2007), operated at much higher Ca.
[13] See EPAPS Document No. E-APPLAB-93-021842. Movie 1 shows oil droplet generated in a restriction channel with dimensions: $h=10$ μm, $w=10$ μm, $l=100$ μm at flow rates of $Q_w=Q_o=0.01$ μL/min. Movie 2 shows oil droplet generated in a restriction channel with dimensions: $h=10$ μm, $w=10$ μm, $l=1000$ μm at flow rates of $Q_w=Q_o=0.0025$ μL/min. For more information on EPAPS, see http://www.aip.org/pubservs/epaps.html.